

# Co-PLNet: A Collaborative Point-Line Network for Prompt-Guided Wireframe Parsing

Chao Wang, Xuanying Li, Cheng Dai, Jinglei Feng, Yuxiang Luo, Yuqi Ouyang and Hao Qin

**Abstract**—Wireframe parsing aims to recover line segments and their junctions to form a structured geometric representation useful for downstream tasks such as Simultaneous Localization and Mapping (SLAM). Existing methods predict lines and junctions separately and reconcile them post-hoc, causing mismatches and reduced robustness. We present Co-PLNet, a point-line collaborative framework that exchanges spatial cues between the two tasks, where early detections are converted into spatial prompts via a Point-Line Prompt Encoder (PLP-Encoder), which encodes geometric attributes into compact and spatially aligned maps. A Cross-Guidance Line Decoder (CGL-Decoder) then refines predictions with sparse attention conditioned on complementary prompts, enforcing point-line consistency and efficiency. Experiments on Wireframe and YorkUrban show consistent improvements in accuracy and robustness, together with favorable real-time efficiency, demonstrating our effectiveness for structured geometry perception. Our code is available at <https://github.com/GalacticHogrider/Co-PLNet>.

**Index Terms**—Attention, Holistic Attraction Field Representation, Line Segment, Mutual Prompt, Wireframe Parsing

## I. INTRODUCTION

Wireframe parsing is a computer vision task that detects line segments in an image to form a structured geometric representation, capturing scene constraints and topological relationships that support robust SLAM [1] [2] [3], scene parsing [4] [5], and high level visual recognition tasks [6]. The interconnections between lines and junctions are important in wireframe parsing, while existing solutions generally utilize these interconnections in a limited way and are thus constrained in performance. As depicted in Fig. 1, traditional paradigms like L-CNN [7] [8] [9] generate massive line proposals and filter them, which is computationally expensive. HAWP [10] [11] recasts sparse line proposals into dense predictions and aligns endpoints with junctions, improving efficiency and accuracy. PLNet [2] builds on HAWP with cascaded U-Net [12] and deep supervision. However, lines

Chao Wang and Xuanying Li contributed equally to this work. (Corresponding author: Yuqi Ouyang).

Chao Wang, Xuanying Li, and Cheng Dai are with the College of Software, Sichuan University, Chengdu 610065, China (email: {2023141461095, 2023141461216}@stu.scu.edu.cn; daicheng@scu.edu.cn).

Jinglei Feng is with the Department of Radiology, North Sichuan Medical College, Nanchong 637000, China (email: jingleifeng82@gmail.com).

Yuxiang Luo is with the Graduate School of Information, Production and Systems, Waseda University, Kitakyushu 808-0135, Japan (email: yuxiang.luo@ruri.waseda.jp).

Yuqi Ouyang is with the College of Computer Science, Sichuan University, Chengdu 610065, China (e-mail: yuqi.ouyang@scu.edu.cn).

Hao Qin is with the School of Electrical and Electronic Engineering, University College Dublin, Dublin, D04 V1W8 Ireland, and also with the School of Electronics and Information Engineering, Sichuan University, Chengdu, 610065, China (e-mail: hao.qin@scu.edu.cn).

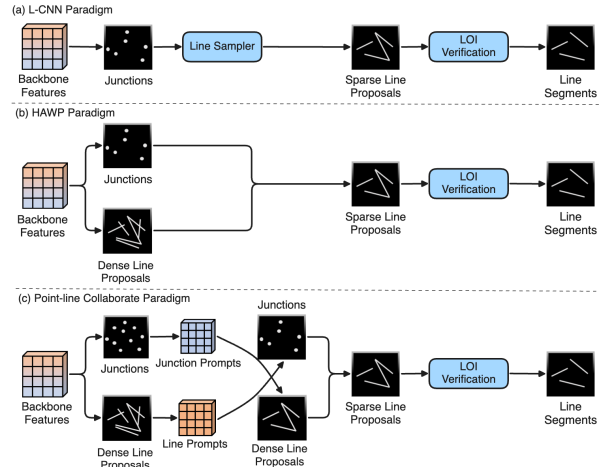


Fig. 1. Conceptual comparison between existing wireframe parsing paradigms and our Co-PLNet. Note that this figure emphasizes architectural differences rather than visual output quality

and junctions are still predicted independently with endpoint adjustments applied afterward, causing potential mismatches between lines and junctions. Such inconsistencies may adversely affect the downstream SLAM tasks that rely on the joint use of both lines and junctions.

To address this bottleneck, we propose the Co-Point Line Net framework named Co-PLNet, which introduces a novel network enabling point-line interaction for wireframe parsing. Depicted in Fig. 1, unlike previous methods that detect lines and junctions separately, our model performs early detection and converts line and junction predictions into spatial prompts, which are exchanged between tasks to enhance point-line consistency. More specifically in Fig. 2, our Point-Line Prompt Encoder (PLP-Encoder) transforms geometric information into structured spatial prompts, supporting the prediction refinement in the Cross-Guidance Line Decoder (CGL-Decoder). Our main contributions are:

- We propose a point-line collaborative paradigm that exchanges spatial prompts between junction and line detection, improving point-line consistency for wireframe parsing.
- We introduce a prompt-based encoding and decoding strategy that effectively fuses line and junction cues, enabling more robust and geometrically consistent predictions.
- Sparse attention is designed within cross-guided decoding to efficiently integrate complementary information, balancing accuracy and real-time performance.

- Comprehensive experiments on the Wireframe and YorkUrban datasets demonstrate our competitive performance.

## II. PROPOSED METHOD

### A. Point-Line Collaborative Paradigm

Existing wireframe parsers predict junctions and lines independently, with post-hoc endpoint adjustment, weakening geometric consistency. We propose a point-line collaborative paradigm that enables bidirectional interaction, yielding geometrically coherent predictions:

$$p(y | I) = \sum_{(y_J, y_L) \in \mathcal{S}(y)} p_J(y_J | I, y_L^{(0)}) \cdot p_L(y_L | I, y_J^{(0)}), \quad (1)$$

where  $I$  denotes the input image,  $y_J^{(0)}$ ,  $y_L^{(0)}$  are coarse spatial prompts from the PLP-Encoder, passed to the CGL-Decoder for final line segment  $y$ .  $\mathcal{S}(y)$  is the set of junction and line proposal pairs  $(y_J, y_L)$ . Conditioning the junction and line prediction tasks  $p_J$  and  $p_L$  on each other's prompts establishes a bidirectional interaction between two tasks, resulting in greater consistency and more reliable geometry.

### B. Point-Line Prompt Encoder

Depicted in Fig. 2, the PLP-Encoder receives the input image and first applies SuperPoint [13] to extract multi-scale features. These are aggregated by a U-Net adopted from PLNet [2] to obtain a refined feature representation. From this refined feature, two lightweight prediction heads together with parsing modules following HAWP [10] produce junction and dense line proposals, respectively. The goal of the PLP-Encoder is to transform these raw geometric predictions into spatial prompts that can guide the second-stage refinement in the CGL-Decoder.

Prior to junction parsing, we follow HAWP [10] and use a point prediction head to predict a junction heatmap  $H_J$  and pixel offsets  $\Delta C_J$ . Let  $C$  denote all pixel coordinates in the image. The junction parsing starts by refining pixel coordinates with the offsets:

$$C_J = C + \Delta C_J. \quad (2)$$

Then, each junction coordinate is assigned with a confidence value by normalizing the heatmap:

$$V_J = \text{softmax}(H_J). \quad (3)$$

After non-maximum suppression (NMS) on the heatmap  $H_J$  and thresholding on confidence  $V_J$ , the junction parsing computes a sparse set of high-confidence junction coordinates  $C_J \in \mathbb{R}^{H \times W \times 2}$ , as geometrically precise junctions.

For line parsing, we follow the HAFM [10] and use the line prediction head to compute the per-pixel scalars  $d, \theta, \theta_1, \theta_2$  together with a small residual  $r$  at every pixel location  $c_i$ . Here  $d$  is the perpendicular distance from  $c_i$  to the associated line segment;  $\theta$  is the segment's tangent orientation that rotates the image axes to the segment-aligned frame;  $\theta_1$  and  $\theta_2$  are endpoint angles measured in the segment-aligned frame

between the perpendicular from  $c_i$  to the segment and the rays pointing toward the two endpoints;  $r$  refines  $d$  for sub-pixel accuracy. Given these quantities, the two endpoints decoded at  $c_i$  are

$$C_{ep} = (d+r) \begin{pmatrix} \cos \theta & -\sin \theta \\ \sin \theta & \cos \theta \end{pmatrix} \begin{pmatrix} 1 & 1 \\ \tan \theta_1 & \tan \theta_2 \end{pmatrix} + [\mathbf{c}_i, \mathbf{c}_i], \quad (4)$$

where  $C_{ep} \in \mathbb{R}^{2 \times 2}$  stores the two endpoint coordinates of the line segment decoded at  $c_i$ . Flattening and evaluating  $C_{ep}$  over all pixel locations in the image produces  $C_L \in \mathbb{R}^{H \times W \times 4}$ , depicting all dense proposals of line segments.

As shown in Fig. 2, after the junction parsing and the line parsing, the junction prompt generator and the line prompt generator transform the junction and line proposals into junction prompts and line prompts, respectively, converting raw geometric predictions into spatial prompts, as follows:

$$y_J^{(0)} = \text{Conv}(\text{ReLU}(\text{Conv}(C_J))), \quad (5)$$

$$y_L^{(0)} = \text{Conv}(\text{ReLU}(\text{Conv}(C_L))), \quad (6)$$

where the kernel sizes of the two convolutions are depicted in Fig. 2. For all the channel settings, we refer to Section III-B. The computations of  $y_J^{(0)}$  and  $y_L^{(0)}$  concludes the PLP-Encoder, resulting in spatially dense prompts that preserve junction density, local connectivity, and line orientation statistics, providing geometry-aware guidance for the refined predictions of line segments  $y$  in the CGL-Decoder, as presented next.

### C. Cross-Guidance Line Decoder

Depicted in Fig. 2, the CGL-Decoder first performs local feature fusion via channel-wise concatenation and convolutional operations of three spatially aligned inputs, they are: the refined feature map  $Z$  produced by the U-Net adopted from PLNet [2], line prompts  $y_L^{(0)}$ , and the junction prompts  $y_J^{(0)}$ , resulting in locally fused features  $\tilde{Z}_L$  and  $\tilde{Z}_J$ .

To capture non-local semantics efficiently, we apply sparse multi-head cross-attention over windowed features  $\tilde{Z}_L$ ,  $\tilde{Z}_J$ , and  $Z$ . A  $1 \times 1$  convolution  $\psi(\cdot)$  first reduces channel dimensions, after which features are partitioned into spatial windows and projected into multiple attention heads. Cross-attention is then performed within corresponding windows across the three feature sources:

$$\bar{Z}_L = \text{MHA}(\psi(\tilde{Z}_L), \psi(Z), \psi(Z)), \quad (7)$$

$$\bar{Z}_J = \text{MHA}(\psi(\tilde{Z}_J), \psi(Z), \psi(Z)), \quad (8)$$

where attended features  $\bar{Z}_L$  and  $\bar{Z}_J$  are produced, which are further injected into the refined representation via gated residual fusion to suppress noise:

$$Z'_L = Z + G_L \odot \bar{Z}_L, \quad Z'_J = Z + G_J \odot \bar{Z}_J, \quad (9)$$

where  $\odot$  denotes element-wise multiplication,  $G_L$  and  $G_J$  are learnable gating masks. The refined features  $Z'_L$  and  $Z'_J$  are used for line and junction prediction, respectively. Prediction

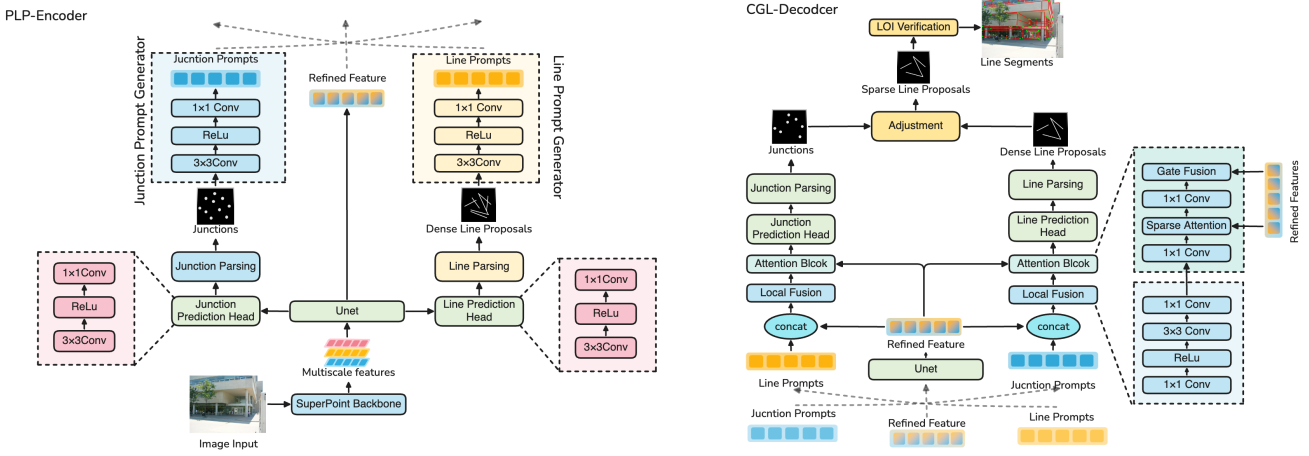


Fig. 2. Overview of the Co-PLNet framework. The PLP-Encoder generates spatial prompts from junction and line predictions, which are refined by the CGL-Decoder to produce accurate line segment predictions.

heads and parsing modules similar to those in the PLP-Encoder are applied to obtain dense line proposals  $y_L$  and junctions  $y_J$ . Following HAWP [2], line endpoints are associated with nearby junctions within a certain threshold and duplicates are removed, yielding sparse line proposals  $y$ . The mutual guidance between line and junction prompts is maintained throughout prediction, enforcing point-line consistency as formalized in Eq. (1). Finally, Line-of-Interest (LOI) verification is applied to  $y$ : features are sampled along each line and scored by an MLP, while the top- $k$  proposals are retained as final predictions. Except the Superpoint module, all components in our solution are trained end-to-end by the following loss:

$$\mathcal{L} = \sum_{m \in \{\text{PLP, CGL}\}} \left( \mathcal{L}_{\text{line}}^{(m)} + \mathcal{L}_{\text{junc}}^{(m)} + \mathcal{L}_{\text{aux}}^{(m)} \right) + \mathcal{L}_{\text{LOI}}, \quad (10)$$

where  $\mathcal{L}_{\text{line}}$  supervises the line parameter maps  $(d, \theta, \theta_1, \theta_2, r)$ ;  $\mathcal{L}_{\text{junc}}$  supervises the junction heatmap and offsets  $(H_J, \Delta C_J)$ ; and  $\mathcal{L}_{\text{aux}}$  enforces geometric consistency between dense line proposals  $C_L$  and the target geometry. The index  $m$  denotes the PLP-Encoder or the CGL-Decoder.  $\mathcal{L}_{\text{LOI}}$  supervises line confidence prediction by aggregating features along each proposal  $y$ . Due to space limitations, the definitions of  $\mathcal{L}_{\text{line}}$ ,  $\mathcal{L}_{\text{junc}}$ , and  $\mathcal{L}_{\text{aux}}$  are not presented here, detailed formulations can be found in [2].

### III. EXPERIMENTS

#### A. Datasets and Evaluation Metrics

Our model is evaluated on the Wireframe [14] and YorkUrban [15] datasets. The Wireframe dataset contains 5,000 training images and 462 test images with richly annotated line segments and junctions from diverse built environments. The YorkUrban dataset includes 102 urban-scene test images and is commonly used to evaluate cross-domain generalization.

We evaluate detection accuracy by structural average precision (sAP), and runtime efficiency using frames per second (FPS). A predicted segment with endpoints  $(\hat{c}_1, \hat{c}_2)$  is considered a true positive if it matches a ground-truth segment with fixed endpoints  $(c_1, c_2)$  satisfying:

$$\|\hat{c}_1 - c_1\|_2^2 + \|\hat{c}_2 - c_2\|_2^2 \leq l. \quad (11)$$

Following [9], we evaluate at thresholds  $l \in \{5, 10, 15\}$  and report sAP<sup>5</sup>, sAP<sup>10</sup>, and sAP<sup>15</sup>. To quantify point-line consistency, we report the endpoint mismatch rate, defined as the percentage of predicted endpoints without a detected junction within 15 pixels.

#### B. Implementation Details

All images are resized to  $512 \times 512$ . Experiments are conducted on an NVIDIA RTX 4080 GPU using PyTorch. The Superpoint module is fixed with the pre-trained version in [13]. Following PLNet [2], we adopt consistent configurations for the backbone, proposal generation, and LOI verification, including 256-channel U-Net features, a 0.008 junction threshold, a 10-pixel proposal range, and the retention of the top-1000 proposals. To balance structural accuracy with real-time efficiency, we employ lightweight configurations for the collaborative modules: both junction and line prompts are encoded with 16 channels, and the sparse multi-head cross-attention projects features to 32 channels using 4 heads with a window size of 8. For training, Adam [16] is used with a learning rate of  $4 \times 10^{-4}$  for 35 epochs, reduced to  $4 \times 10^{-5}$  for the final 5 epochs. The batch size is set to 6.

#### C. Comparison with SOTA Methods

To comprehensively evaluate our performance, we conducted extensive comparisons with state-of-the-art (SOTA) approaches on the two datasets. Tabulated in Table I, for both color and greyscale inputs, our method consistently outperforms prior work across all sAP thresholds on both datasets, while maintaining a real-time efficiency at 76.8 FPS. Visual comparisons in Fig. 3 highlight the improvements of our framework. Compared with F-Clip, HAWPv2, and PLNet, Co-PLNet produces more complete and geometrically consistent line-junction structures, closely matching the ground truth annotations. These findings establish Co-PLNet as a competitive approach for accurate and efficient wireframe parsing.

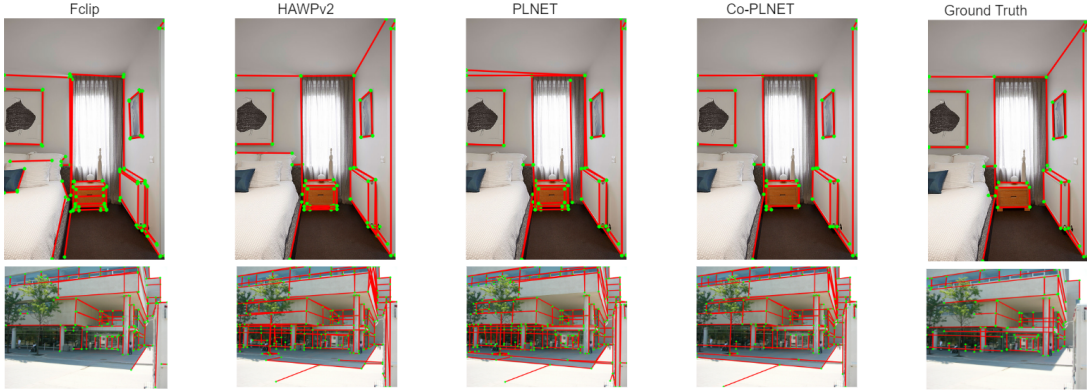


Fig. 3. Visualization of parsing results. The first and second rows show images from the Wireframe and YorkUrban datasets, respectively, with predicted wireframes aligned to ground-truth annotations.

TABLE I  
PERFORMANCE COMPARISON ON THE WIREFRAME AND YORKURBAN DATASETS. RESULTS ARE REPORTED FOR COLOR INPUTS, WHILE METHODS MARKED WITH <sup>\*</sup> CORRESPOND TO GRAYSCALE INPUTS. THE HIGHEST RESULT IS IN **BOLD**, AND THE SECOND HIGHEST IS UNDERLINED

Methods	Wireframe			YorkUrban			FPS
	sAP <sup>5</sup>	sAP <sup>10</sup>	sAP <sup>15</sup>	sAP <sup>5</sup>	sAP <sup>10</sup>	sAP <sup>15</sup>	
AFM [17]	18.5	24.4	27.5	7.3	9.4	11.1	10.4
AFM++ [17]	27.7	32.4	34.8	9.5	11.6	13.2	8.0
L-CNN [9]	59.7	63.6	65.3	25.0	27.1	28.3	29.6
LETTR [8]	59.2	65.2	67.7	23.9	27.6	29.7	2.0
F-Clip [7]	64.3	68.3	69.1	28.6	31.0	32.4	82.3
ELSD [18]	64.3	68.9	70.9	27.6	30.2	31.8	42.6
HAWPv2 [11]	<u>65.7</u>	<u>69.7</u>	<u>71.3</u>	28.9	<u>31.2</u>	<u>32.6</u>	<b>85.2</b>
Co-PLNet	<b>68.4</b>	<u>72.3</u>	<u>73.8</u>	<u>32.7</u>	<u>35.6</u>	<u>36.6</u>	76.8
<sup>*</sup> HAWPv2 [11]	63.6	67.7	69.5	26.6	29.0	30.3	<b>85.2</b>
<sup>*</sup> PLNet [2]	<u>65.2</u>	<u>69.2</u>	<u>70.9</u>	<u>29.3</u>	<u>32.0</u>	<u>33.5</u>	<u>79.4</u>
<sup>*</sup> Co-PLNet	<b>67.9</b>	<u>71.7</u>	<u>73.3</u>	<u>32.3</u>	<u>35.3</u>	<u>36.4</u>	76.8

TABLE II

ABLATED PERFORMANCE UNDER DIFFERENT SYSTEM CONFIGURATIONS. PL AND LP DENOTE POINT-TO-LINE AND LINE-TO-POINT PROMPTS; LF IS LOCAL FEATURE FUSION; SA IS SPARSE ATTENTION; DA IS DENSE ATTENTION. MIS. INDICATES THE ENDPOINT MISMATCH RATE (%).

PL	LP	LF	SA	DA	Wireframe			YorkUrban			FPS	
					sAP <sup>5</sup>	sAP <sup>10</sup>	sAP <sup>15</sup>	Mis.↓	sAP <sup>5</sup>	sAP <sup>10</sup>	sAP <sup>15</sup>	
✓	✓				65.2	69.2	70.9	12.4	29.3	32.0	33.5	13.1 79.4
					66.1	70.3	72.3	11.2	30.1	32.7	34.8	12.0 78.5
✓	✓				66.8	70.4	71.5	10.8	30.8	32.5	33.9	11.5 78.3
✓	✓	✓			67.1	71.2	72.6	9.6	31.4	33.9	35.1	10.2 77.6
✓	✓	✓	✓		67.9	71.7	73.3	7.8	32.3	35.3	36.4	8.5 76.8
✓	✓	✓	✓	✓	68.1	71.9	73.6	7.5	32.5	35.5	36.7	8.2 42.1

#### D. Ablation Study

We evaluate different model components on Wireframe and YorkUrban, with input images converted to greyscale. As summarized in Table II, the baseline, without prompts, local fusion (LF), or sparse attention (SA), achieves sAP at 65.2, 69.2, 70.9 on Wireframe and 29.3, 32.0, 33.5 on YorkUrban. Introducing the point-to-line (PL) prompt improves line-proposal quality and point-line connectivity, enhancing accuracy especially at sAP<sup>15</sup>, while the line-to-point (LP) prompt focuses on refining junction localization, therefore limited at boosting sAP<sup>5</sup>. Enabling both prompts jointly increases precision further and reduces endpoint mismatch (Mis.) from 12.4 to 9.6 on Wireframe, demonstrating the complementary benefits of

TABLE III  
PERFORMANCE IMPACT OF WINDOW SIZE  $w$  FOR SPARSE ATTENTION.

Window Size	Wireframe			YorkUrban			FPS
	sAP <sup>5</sup>	sAP <sup>10</sup>	sAP <sup>15</sup>	sAP <sup>5</sup>	sAP <sup>10</sup>	sAP <sup>15</sup>	
4	67.2	71.3	72.8	31.1	34.7	35.8	<b>78.4</b>
8	<b>67.9</b>	<b>71.7</b>	<b>73.3</b>	<b>32.3</b>	<b>35.3</b>	<b>36.4</b>	76.8
16	67.6	71.5	73.1	31.9	35.1	36.1	74.2

mutual point-line prompting. Furthermore, adding SA in the CGL-Decoder provides additional gains, whereas replacing it with dense attention marginally improves sAP<sup>15</sup> but drops FPS from 76.8 to 42.1, justifying the sparse design. Overall, these results highlight that each component contributes to more accurate junctions and better line connectivity while keeping the system real-time.

#### E. Parameter Study

Table III investigates the impact of window size for sparse attention, using Wireframe and YorkUrban images converted to greyscale. All scoring metrics follow a consistent trend, peaking at a window size of 8 across both datasets. A smaller window size of 4 increases inference speed but reduces precision, while increasing the window size to 16 does not improve accuracy and adds computational overhead. These observations justify 8 as the optimal window size in sparse attention for balancing accuracy and efficiency.

#### IV. CONCLUSION

We present Co-PLNet, a prompt-based collaborative framework for wireframe parsing that tightly integrates line and junction prediction. Preliminary junction and line predictions are converted into spatial prompts by the PLP-Encoder and exchanged in the CGL-Decoder via sparse attention, enhancing point-line consistency and achieving competitive structural average precision on the Wireframe and YorkUrban datasets, while operating at 76.8 FPS. Ablation studies further confirm the effectiveness of each model component, particularly the spatial prompts that provide mutual guidance. Future work will extend this framework to wireframe parsing in closed-loop SLAM scenarios.

## REFERENCES

- [1] K. Xu, Y. Hao, S. Yuan, C. Wang, and L. Xie, "Airvo: An illumination-robust point-line visual odometry," in *2023 IEEE/RSJ International Conference on Intelligent Robots and Systems (IROS)*, 2023, pp. 3429–3436.
- [2] ——, "Airslam: An efficient and illumination-robust point-line visual slam system," *IEEE Transactions on Robotics*, 2025.
- [3] L. Liu, H. Li, H. Yao, and R. Zha, "Pluckernet: Learn to register 3d line reconstructions," in *Proceedings of the IEEE/CVF Conference on Computer Vision and Pattern Recognition*, 2021, pp. 1842–1852.
- [4] Y. N. Wu, Z. Si, H. Gong, and S.-C. Zhu, "Learning active basis model for object detection and recognition," *International journal of computer vision*, vol. 90, no. 2, pp. 198–235, 2010.
- [5] L. Duan and F. Lafarge, "Image partitioning into convex polygons," in *Proceedings of the IEEE Conference on Computer Vision and Pattern Recognition*, 2015, pp. 3119–3127.
- [6] J. Lazarow, W. Xu, and Z. Tu, "Instance segmentation with mask-supervised polygonal boundary transformers," in *Proceedings of the IEEE/CVF Conference on Computer Vision and Pattern Recognition*, 2022, pp. 4382–4391.
- [7] X. Dai, H. Gong, S. Wu, X. Yuan, and Y. Ma, "Fully convolutional line parsing," *Neurocomputing*, vol. 506, pp. 1–11, 2022.
- [8] Y. Xu, W. Xu, D. Cheung, and Z. Tu, "Line segment detection using transformers without edges," in *Proceedings of the IEEE/CVF Conference on Computer Vision and Pattern Recognition*, 2021, pp. 4257–4266.
- [9] Y. Zhou, H. Qi, and Y. Ma, "End-to-end wireframe parsing," in *Proceedings of the IEEE/CVF International Conference on Computer Vision*, 2019, pp. 962–971.
- [10] N. Xue, T. Wu, S. Bai, F. Wang, G. Xia, L. Zhang, and P. H. S. Torr, "Holistically-attracted wireframe parsing," in *Proceedings of the IEEE/CVF Conference on Computer Vision and Pattern Recognition*, 2020, pp. 2788–2797.
- [11] ——, "Holistically-attracted wireframe parsing: From supervised to self-supervised learning," *IEEE Transactions on Pattern Analysis and Machine Intelligence*, vol. 45, no. 12, pp. 14 727–14 744, 2023.
- [12] O. Ronneberger, P. Fischer, and T. Brox, "U-net: Convolutional networks for biomedical image segmentation," in *International Conference on Medical image computing and computer-assisted intervention*. Springer, 2015, pp. 234–241.
- [13] D. DeTone, T. Malisiewicz, and A. Rabinovich, "Superpoint: Self-supervised interest point detection and description," in *Proceedings of the IEEE conference on computer vision and pattern recognition workshops*, 2018, pp. 224–236.
- [14] K. Huang, Y. Wang, Z. Zhou, T. Ding, S. Gao, and Y. Ma, "Learning to parse wireframes in images of man-made environments," in *Proceedings of the IEEE Conference on Computer Vision and Pattern Recognition*, 2018, pp. 626–635.
- [15] P. Denis, J. H. Elder, and F. J. Estrada, "Efficient edge-based methods for estimating manhattan frames in urban imagery," in *European conference on computer vision*. Springer, 2008, pp. 197–210.
- [16] D. P. Kingma and J. Ba, "A method for stochastic optimization," *arXiv preprint arXiv:1412.6980*, vol. 1412, no. 6, 2014.
- [17] N. Xue, S. Bai, F. Wang, G. Xia, T. Wu, and L. Zhang, "Learning attraction field representation for robust line segment detection," in *Proceedings of the IEEE/CVF Conference on Computer Vision and Pattern Recognition*, 2019, pp. 1595–1603.
- [18] H. Zhang, Y. Luo, F. Qin, Y. He, and X. Liu, "Elsd: Efficient line segment detector and descriptor," in *Proceedings of the IEEE/CVF International Conference on Computer Vision*, 2021, pp. 2969–2978.